Effect of glass–ceramic microstructure on its *in vitro* bioactivity

P. N. DE AZA
Instituto de Bioingeniería, Universidad Miguel Hernandez de Elche, Edificio Torrevaillo Avda, Ferrocarril s/n 03202-Elche, Alicante, Spain
E-mail: piedad@umh.es

Z. B. LUKLINSKA
Materials Department, Queen Mary University of London, Mile End Road, London E1 4NS, UK

Two routes were used to obtain a glass–ceramic composed of 43.5 wt % SiO_2 – 43.5 wt % CaO – 13 wt % ZrO_2. Heat treatment of a glass monolith produced a glass–ceramic (WZ1) containing wollastonite-2M and tetragonal zirconia as crystalline phases. The WZ1 did not display bioactivity *in vitro*. Ceramizing the glass via powder technology routes formed a bioactive glass–ceramic (WZ2). The two glass–ceramics, WZ1 and WZ2, were composed of the same crystalline phases, but differed in microstructure. The *in vitro* studies carried out on WZ2 showed the formation of an apatite-like layer on its surface during exposure to a simulated body fluid. This paper examined the influence of both chemical and morphological factors on the *in vitro* bioactivitity. The interfacial reaction product was examined by scanning and transmission electron microscopy. Both instruments were fitted with energy-dispersive X-ray analyzers. Measurements of the pH made directly at the interface of the two glass–ceramics were important in understanding their different behavior during exposure to the same physiological environment.

1. Introduction

A surgical implant may be defined as an object comprising non-living materials introduced into the human body and designed to fulfil a specific function over a specified time span [1, 2]. Basically, the important properties of a material can be classified into four categories: mechanical, physical, chemical and biological. Physical and mechanical properties control the active functional characteristics of most implants, while chemical and biological properties control the ability of the implant to maintain its functionality throughout the implantation time. The material selection, based on the properties required for the application and characteristics of the materials, determines the functional suitability of the implant.

There has been an increasing interest in bioactive glass and glass–ceramics in the past two decades, due to their critical structural application within the human body, mainly as bone bonding and bone substitute materials [3–10]. The behavior of these groups of materials has usually been related to their chemical composition, but a careful study of their microstructure appears equally important in order to understand their properties in the physiological environment. This last point is particularly interesting in the case of bioactive ceramics, glasses and glass–ceramic materials, which showed the ability of developing a strong bond to natural bone tissue after their implantation into animal and human bodies [11–15]. Several authors [16–19] have described the bonding mechanism as a sequence of reactions between the glass and glass–ceramic with the surrounding fluid. In most instances, a silicon-rich layer was initially observed followed by the formation of a calcium–phosphate-rich layer [20–24].

Since the discovery of bioglasses by Hench *et al*. [25] in the early 1970s, various types of ceramics, glasses and glass–ceramics have been used as bone replacement materials [26, 27]. Most of them are based in the $CaO–MgO–P_2O_5–SiO_2$ system [28–34]. Small amounts of other constituents like CaF_2 or TiO_2 had also been added to the initial composition, in order to facilitate glass processing.

Natural bones and teeth are multiphase materials, thus their combined properties are likely to be reproduced by multiphase materials. Although composite fabrication appears as a possibility to create such materials, crystallization of glasses seems to be a very effective way to simulate hard tissue in these applications.

In this study, a glass of the $SiO_2 \cdot CaO–ZrO_2$ system was processed by two dissimilar routes, in order to obtain two different microstructures with the same glass–ceramic composition. First, by heat treatment of a glass monolith, a WZ1 glass–ceramic was obtained. Second, by ceramizing the glass via a powder technology route

similar to that employed for ceramics which eliminates the formation of cracks in the glass ceramic specimen, a WZ2 glass–ceramic was obtained. The main objective was to examine the influence of both chemical and morphological factors on the reactivity of the glass–ceramics in a simulated body fluid (SBF). Changes in pH at the glass–ceramic/SBF interface were measured. It was important to record this parameter, as it was indicative of the chemical changes taking place directly at the interface. The product of the interfacial reactions was examined by scanning and transmission electron microscopy (SEM and TEM). The chemistry of the interfaces was analyzed using energy dispersive X-ray spectroscopy (EDS). X-ray spectra and elemental maps were obtained when viewing images in secondary and back scattered electron modes.

2. Materials and methods

The pseudobinary system $CaO \cdot SiO_2$–ZrO_2 shows a peritectic invariant point at $1467^\circ \pm 2\,^\circ C$ [35]. In this study, a glass composition corresponding to 87 wt % $CaO \cdot SiO_2$–13 wt % ZrO2 was chosen, as it represents the only composition in the system characterised by the lowest melting temperature.

The starting materials composed of high-purity ZrO_2 (99.99 wt % with low Hf content) and pseudowollastonite (the high temperature polymorph of the chain-silicate mineral wollastonite) were synthesized by a solid state reaction at 1500 °C for 4 h from a stoichiometric mixture of calcium carbonate (99.5 wt %) and high purity washed Belgian sand (99.9 wt %). Details of pseudowollastonite preparation and characterization can be found in previous publications [36, 37].

At first, the powders were separately ground to a particle size < 30 m. Next, the desired proportions of the constituents were weighed out and thoroughly mixed with the help of a small addition of acetone in a manual agate mortar. In order to remove the volatile components, the mixture was dried at 100 °C.

The dried powder was heat treated up to 1550 °C, which was 83 °C over the peritectic point temperature. This process allowed a material of sufficiently low viscosity to be produced, so that it could be poured out onto a metal plate, avoiding at the same time any possibility of devitrification. The processing time was 3 h, sufficient to obtain a good homogenization of the melt. Afterwards, the melt was quenched in water.

The dried glass powder underwent differential thermal analysis (DTA) at a heating rate of 10 °C/min, starting at room temperature up to 1500 °C. The test was carried out in a platinum crucible and under atmospheric conditions. DTA results established the temperatures at which the crystalline phases formed and their possible polymorphic transformations. Based on the DTA results, several heat treatments were performed in order to obtain glass–ceramics of desired composition.

The glass–ceramic WZ1 was obtained by remelting the glass powder at 1550 °C over 3 h in a platinum crucible, followed by casting the melt on a metal plate. Next, the glassy block was annealed at 875 °C and slowly cooled down to room temperature, in order to eliminate the stress formed during the cooling process. Finally, the glass–ceramic WZ1 underwent a heat treatment at 1100 ° for 1 h.

A crack-free glass–ceramic (WZ2) was obtained by grinding the glass block in an attrition mill until the particles passed through a 30 μm sieve. The material was then isostatically pressed into a bar shape at 200 MPa. Pellets were obtained from the bars and heat treated at 1100 °C for 1 h.

Samples of the glassy block WZ1 and glass–ceramic WZ2 were studied by X-ray diffraction (XRD) using a Siemens D-5000 instrument. The microstructures of the WZ1 and WZ2 glass–ceramics were first examined by conventional scanning electron microscopy (SEM) at 15 kV using a Jeol JSM6300 model, fitted with EDS.

The WZ1 and WZ2 glass–ceramics were cut by a low-speed diamond disc to prismatic pieces of $5 \times 5 \times 2\,mm^3$ dimensions. These specimens were immersed in 100 ml of SBF at human body temperature (36.6 °C) in polyethylene bottles [38]. The immersion period of the material in SBF was up to 4 weeks. The choice of this time span was based on the results obtained from previous *in vitro* experiments performed in the same media [39–41]. Changes in pH at the glass–ceramics-SBF interface were determined daily using an ion-sensitive field-effect transistor (ISFET-meter) of Si_3N_4 type [42, 43]. The superficial changes of the glass–ceramics and the morphology of the polished cross sections of the exposed specimens to SBF were first studied in the SEM by secondary electron imaging, followed by EDS analysis. The samples were prepared to a 1 μm diamond paste finish, ultrasonically cleaned in distilled water and thoroughly dried in air prior to carbon coated.

The surface reaction product was examined using a high resolution TEM, Jeol JEM 2010 fitted with LaB_6 filament at 200 keV. Specimens for the study were prepared by dispersing the powder removed from the exposed surfaces in a Petri dish filled with methanol. The wet powder was picked up directly on carbon coated TEM cooper grids of 200 mesh and coated with a thin layer of carbon. Electron beam transparent particles were chosen for TEM examination and examined by selected area diffraction (SAD), low and high magnification imaging, and EDS.

3. Results

The XRD pattern of the original, as-manufactured glass block (Fig. 1) did not display any diffraction peaks confirming the amorphous state of the sample. The DTA results of the glass powder are shown in Fig. 2. A small endothermic effect was observed at around 845 °C, which was attributed to the softening of the glass ($T_r = 845\,^\circ C$). Thus, the temperature of 875 °C was chosen for annealing of the glass block. A strong exothermic effect observed at around 980 °C with a small shoulder around 960 °C were attributed to the crystallization of tetragonal zirconia and wollastonite-2M, respectively. This finding was confirmed by XRD analysis of the quenched sample from 1050 °C (Fig. 3). The small endothermic effect at $\sim 1250\,^\circ C$ was due to the polymorphic transformation of wollastonite-2M into pseudowollastonite (Fig. 3). Finally, a strong

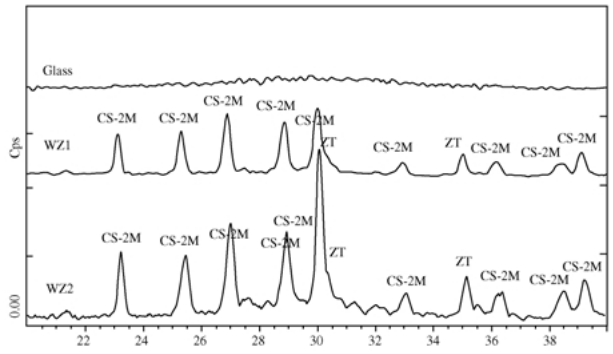

Figure 1 X-ray diffraction spectra of the glass and the WZ1 and WZ2 glass–ceramics, both heated at 1100 °C for 1 h. CS-2M, wollastonite-2M; ZT, tetragonal zirconia.

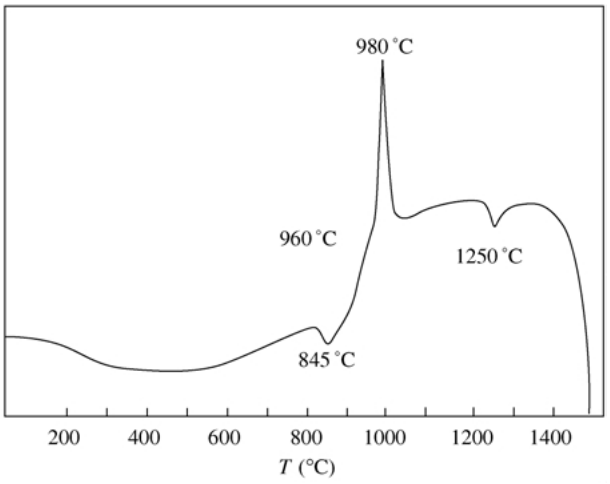

Figure 2 DTA of the glass.

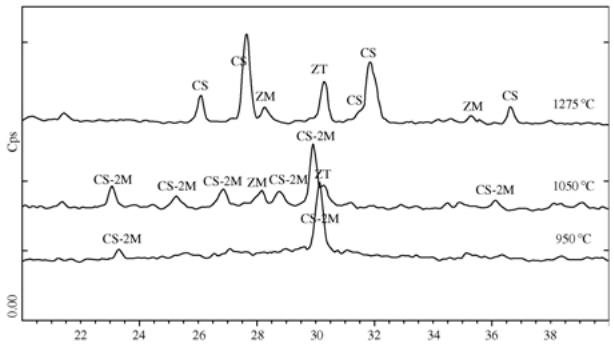

Figure 3 XRD of the glass over the diverse range of processing temperatures. CS-2M, wollastonite-2M; CS, pseudowollastonite; ZT, tetragonal zirconia; ZM, monoclinic zirconia.

endothermic effect occurred at $\sim 1460\,^{\circ}C$ which was attributed to the initial melting of the glass, and agreed with the temperature of the peritectic point of the pseudobinary system $CaO \cdot SiO_2$–ZrO_2 [35].

Fig. 3 shows the XRD patterns obtained from the glass over the diverse range of processing temperatures. A partial devitrification occurred at around 950 °C due to the nucleation of wollastonite-2M phase. As soon as the temperature increased, the degree of material crystallinity had also increased. A certain number of peaks corresponding to the monoclinic zirconia appeared as a result of its partial tetragonal transformation to the

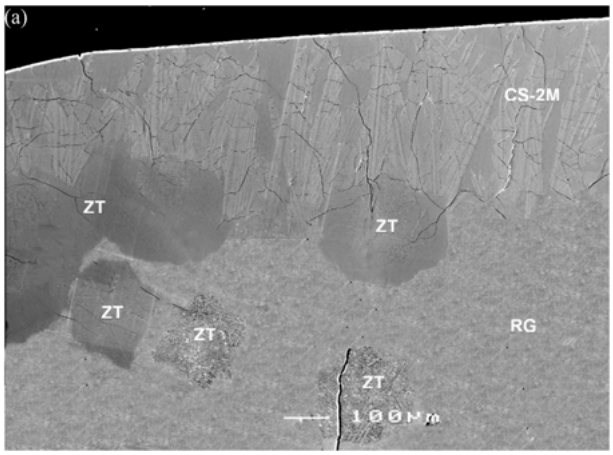

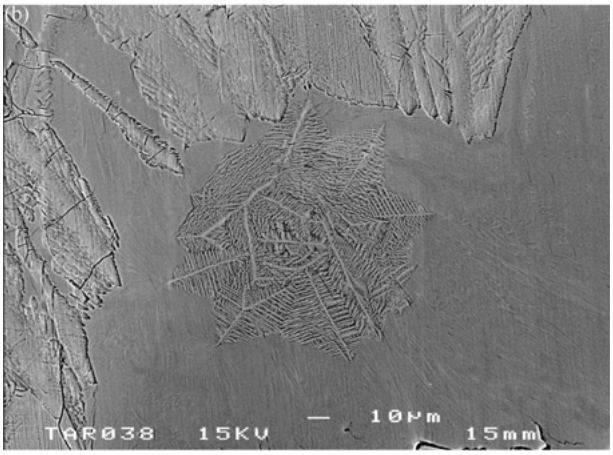

Figure 4 Microstructure of the WZ1 glass–ceramic, (a) SEM image at low magnification. CS-2M, wollastonite-2M; ZT, tetragonal zirconia; RG, residual glass, (b) close up of the SEM image.

monoclinic form which occurred when the samples were ground in preparation for the XRD analysis.

The XRD patterns of the WZ1 and WZ2 (Fig. 1) showed that both glass–ceramics were composed of wollastonite-2M and tetragonal zirconia.

SEM observation of WZ1 clearly showed that the devitrification of the glass block occurred by segregation of the two phases. Fig. 4(a) shows the wollastonite-2M phase in shape of thin fibers radiating from the outer part of the pellet to its center, while the tetragonal zirconia phase precipitated in the inner part of the pellet. The zones of the gray color corresponded to the residual glass, which did not devitrified. A closed up observation of the tetragonal zirconia precipitations (Fig. 4(b)) showed that they were formed of nearly equiaxial rosettes, with an average diameter of $\approx 150 \pm 10\,\mu m$. The rosettes contained alternating radial dendrites of tetragonal zirconia phase (white contrast) and dendrites of wollastonite-2M phase (dark contrast).

Fig. 5 shows a secondary electron image at low magnification of the microstructure of a crack-free polished surface of glass–ceramic WZ2. This microstructure was characterized by a regular devitrification containing closed round pores of a medium size of $\approx 10\,\mu m$.

The pH measurements, recorded directly at the interface of the WZ2 specimen with the SBF solution,

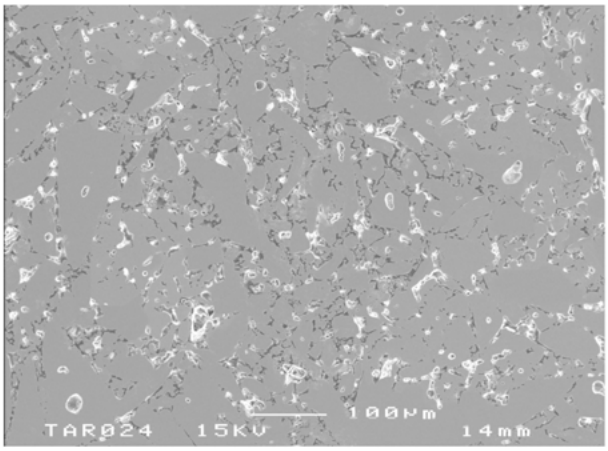

Figure 5 SEM image showing the microstructure of the WZ2 glass–ceramic.

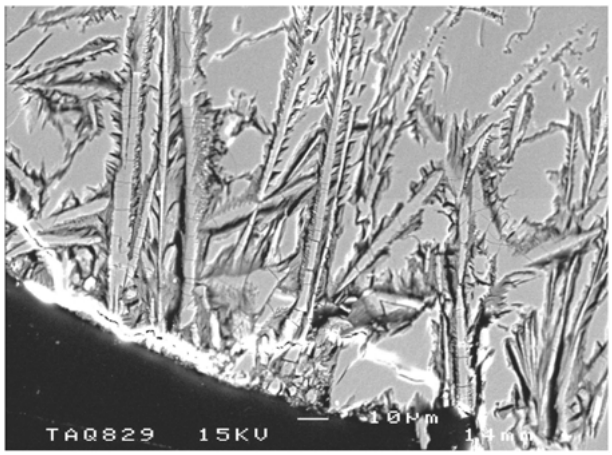

Figure 7 SEM image of a cross-section microstructure of the WZ1 glass–ceramic after 1 month immersion in SBF.

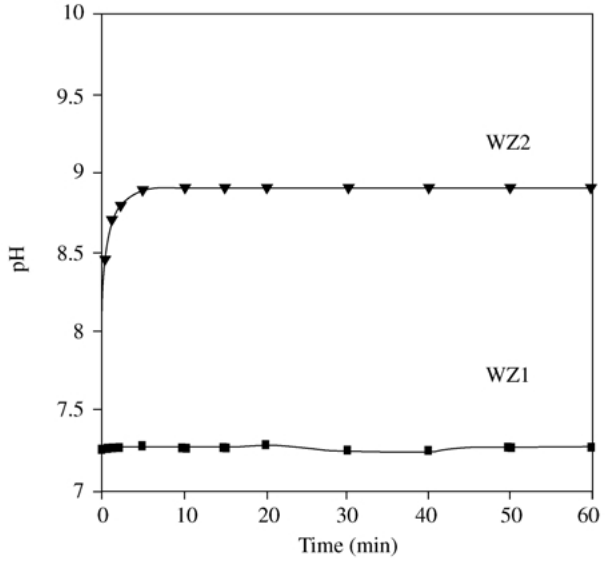

Figure 6 Changes in pH recorded at the interface of the glass–ceramics/SBF.

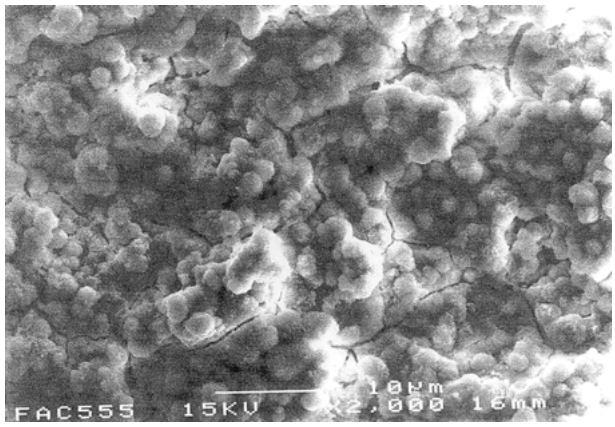

Figure 8 The microstructure of the WZ2 glass–ceramic surface after 1 month immersion in SBF showing globular HA-like phase.

increased sharply from 7.25 to 8.9 in the first 5 min of immersion. After this time, the pH stabilized and remained unchanged at the maximum-recorded value of 8.9. Over the same period of time, the pH at the interface with WZ1 fluctuated at a near-constant value of 7.25 (Fig. 6).

In contrast to the WZ2 specimen, there were no morphological changes observed on the surface of the WZ1 material after the one month exposure period to SBF. To demonstrate this point, Fig. 7 shows the microstructure of the polished cross-section observed under the SEM. Therefore, the *in vitro* study in SBF demonstrated the inability of the WZ1 to form a CaO/P_2O_5-rich surface layer.

The surface of the WZ2 material after one month immersion in SBF contained an HA-like phase with characteristic globular morphology as shown in Fig. 8. The globules formed a compact and continuous layer. The cracks visible in the figure are artifacts caused by drying of the specimen in air.

Fig. 9 shows a representative microstructure of the polished cross-section of the WZ2 glass–ceramic after one month immersion in SBF, and its relevant X-ray maps for silicon, calcium and phosphorous elements. This compositional microcharacterization of the interface showed that the reaction zone was composed of two chemically dissimilar layers formed on the glass–ceramic surface. The outer layer, with an average thickness of about 10 µm, was composed of a CaO/P_2O_5-rich phase, while the much thinner underlayer (about 1/10 of the thickness of the outer layer) in direct contact with the WZ2 substrate, was rich in silicon but depleted in calcium.

The TEM technique was used to examine the ultrastructure of the surface product formed after the exposure of the WZ2 sample to SBF for one month. The characteristic plate-like morphology of the HA-like surface product at low magnification is shown in Fig. 10(a). EDS analysis performed on these thin crystals confirmed the presence of calcium and phosphorous in this region (Fig. 10(b)). High-resolution lattice imaging of the HA-like crystals indicated that the individual crystals formed a continuous phase by growing in direct contact with each other. Images of (0 0 2) lattice planes with 0.344 nm spacing were well resolved in many areas (Fig. 10(c)), and these appeared to be defect free. The measured lattice spacing from the negatives matched well with the values for HA reported in the literature [44–

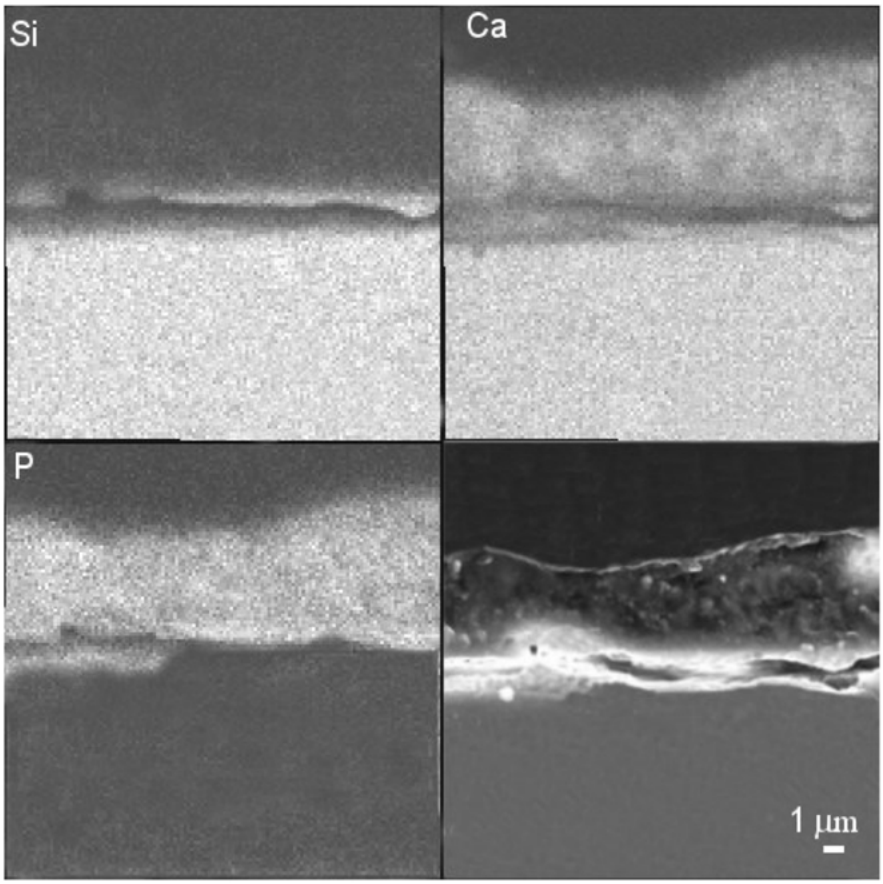

Figure 9 X-ray elemental maps of Si, Ca, P, and a relevant SEM image of the cross-section of the WZ2 glass–ceramic after 1 month immersion in SBF.

48]. When the specimen was appropriately oriented, the selected area diffraction pattern displayed a sharp and continuous ring of (1 1 1) planes corresponding to the 0.388 nm spacing. In addition, a sharp arc doublet of (0 0 2) planes related to the 0.344 nm lattices was also present, indicating the preferential orientation of the HA-like crystals in the layer (Fig. 10(d)).

The intermediate layer was found to be physically continuous at a high magnification level. The SAD pattern of this region showed that the phase was amorphous (Fig. 11(a)). EDS analysis identified the presence of SiO_2 in the layer (Fig. 11(b)).

4. Discussion

The *in vitro* results carried out in SBF for the two glass–ceramics; WZ1 obtained by heat treatment of a glass block, and WZ2 obtained by a combined sintering–devitrification processing of the powdered glass, concluded that each material displayed different *in vitro* behavior in SBF.

WZ1 was not able to form a calcium phosphate layer after one month in SBF. Its surface morphology remained unchanged as observed by the SEM study of the polish cross-section. Also, the pH measurements performed directly at the interface recorded constant values throughout the whole exposure period. Thus, these observations dismissed the WZ1 material as being bioactive. On the other hand, WZ2 showed a high reactivity with the SBF, forming a well-defined HA-like layer on its surface over the same immersion time. In this case, the pH at the interface significantly increased from the initial value recorded immediately after the SBF immersion, indicating changes associated with the surface bioactive behavior. SEM and TEM studies including X-ray elemental maps also confirmed characteristic chemical and structural changes associated with the bioactivity.

The dissimilar behavior of WZ1 and WZ2 in SBF appeared to be related to morphological and chemical differences between the two glass–ceramics.

Overall the results suggested that the mechanism of HA-like phase formation on WZ2 in SBF was similar to that observed on silica-based and crystalline bioactive materials [39, 41]. It was found that the HA-like layer precipitated from the SBF medium onto the amorphous silica intermediate layer was due to the high pH conditions ($pH = 8.9$) developed at the WZ2/SBF interface. The increase in the pH reading resulted from the ionic exchange of Ca^{++}, released from the wollastonite-2M network, for $2H_3O^+$ from the SBF.

Selected area diffraction performed in the TEM showed that the crystallography of the newly formed HA-like particles was similar to the mineral constituent of cortical bone [49–51].

In WZ1, the formation of a heterogeneous microstructure containing wollastonite-2M and tetragonal zirconia as crystalline phases, produced a residual glassy phase of modified composition with regard to the parent glass. Depletion of Ca^{++} in the residual glass by crystallisation of wollastonite-2M during the heat treatment might have chemically stabilized the material,

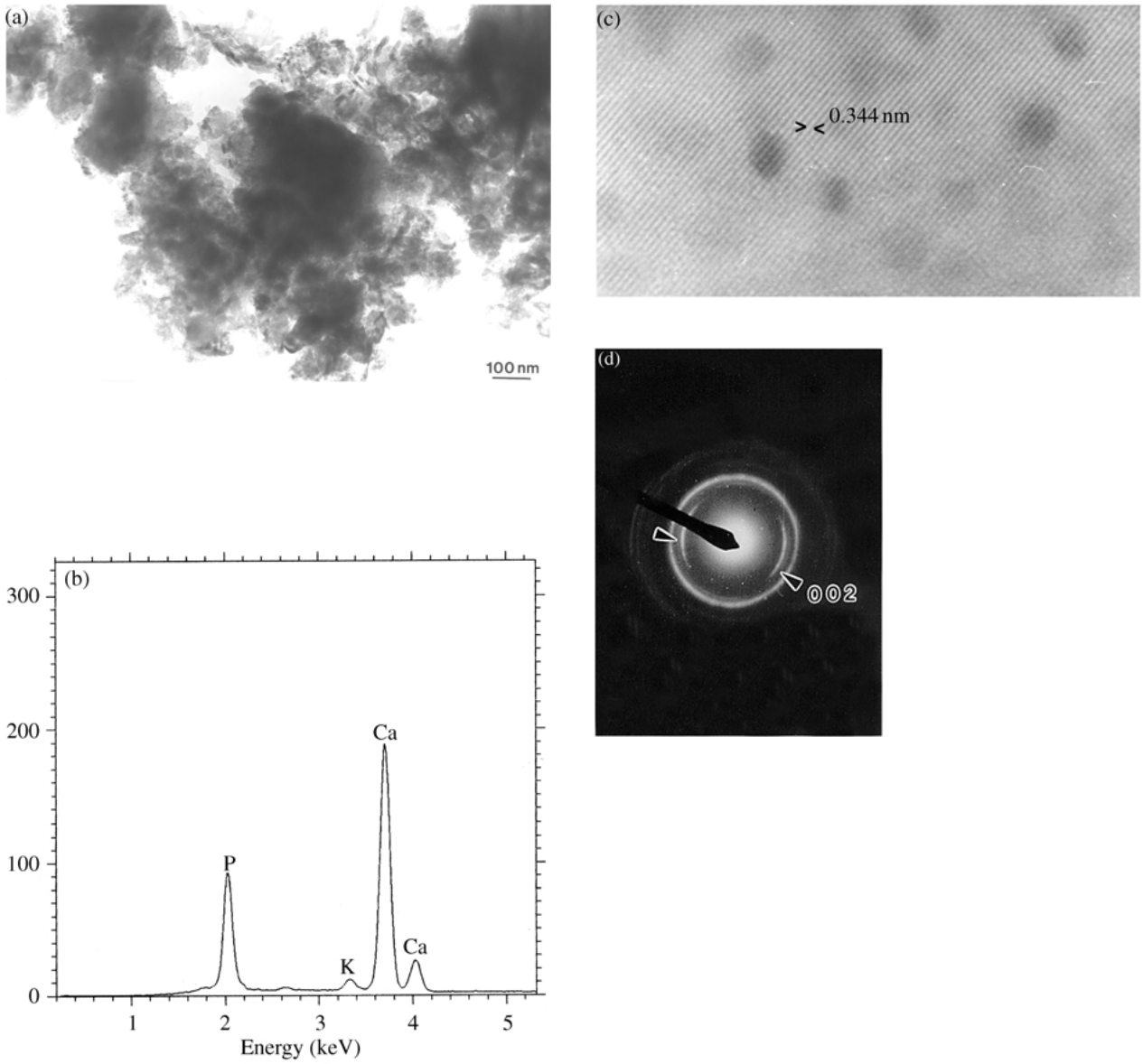

Figure 10 (a) TEM image of the surface product formed on WZ2 glass–ceramic after 1 month in SBF, (b) EDS analysis of the area, (c) high-resolution TEM image of the HA crystals formed on WZ2 glass–ceramic after 1 month exposure to SBF, (d) selected area diffraction pattern of the region.

thus hindering the ionic exchange of Ca^{++} from the wollastonite-2M network for $2H_3O^+$ from the SBF. This was confirmed by the constant pH value ($pH = 7.25$), recorded directly at the WZ1/SBF interface over the immersion time in SBF solution. This behavior was in agreement with the results obtained in previous research carried out on different glasses as well as glass–ceramics with polyvalent metal contents [52–54].

WZ1 displayed a microstructure with a high concentration of Zr^{4+} ions in the center of the material. Such a material was likely to loose its bioactivity due to the formation of oxide and/or hydroxide multilayers on its surface. A solubility limit of these multilayers needed lower pH, that those required for the formation of the HA layer. This effect stabilized the multilayers, making the material inert. Gross *et al*. [52–54] also reported this fact; that the addition of elements such as Al^{3+}, Zr^{4+}, Ta^{5+}, Ti^{4+} etc. into glasses or glass–ceramics eliminates their bioactivity by the formation of multilayers of oxides, hydroxides, and multivalent layers composed of metal carbonates on the surface of the materials.

5. Conclusions

By making use of the $CaO \cdot SiO_2$–ZrO_2 system, a parent glass was obtained from which two glass–ceramics with different microstructures were developed. By heat treatment of the glass, a glass–ceramic (WZ1) containing wollastonite-2M and tetragonal zirconia as the crystalline phases, was obtained. The manufactured WZ1 did not show *in vitro* bioactive properties.

Another glass–ceramic called WZ2 was obtained by sintering–devitrification of the glass. This material contained the same crystalline phases as glass–ceramic WZ1, but demonstrated a very different microstructure.

The study proved the high reactivity of the WZ2 glass–ceramic in a simulated body fluid for a period of one month. The HA-like layer formed at the interface was found to be compact, continuous and composed of many small crystallites, whose ultrastructure resembled natural cortical bone and dentine.

It was important to confirm that the high pH conditions ($pH = 8.9$) existing directly at the WZ2/SBF interface were essential to promote HA-like precipitation. This

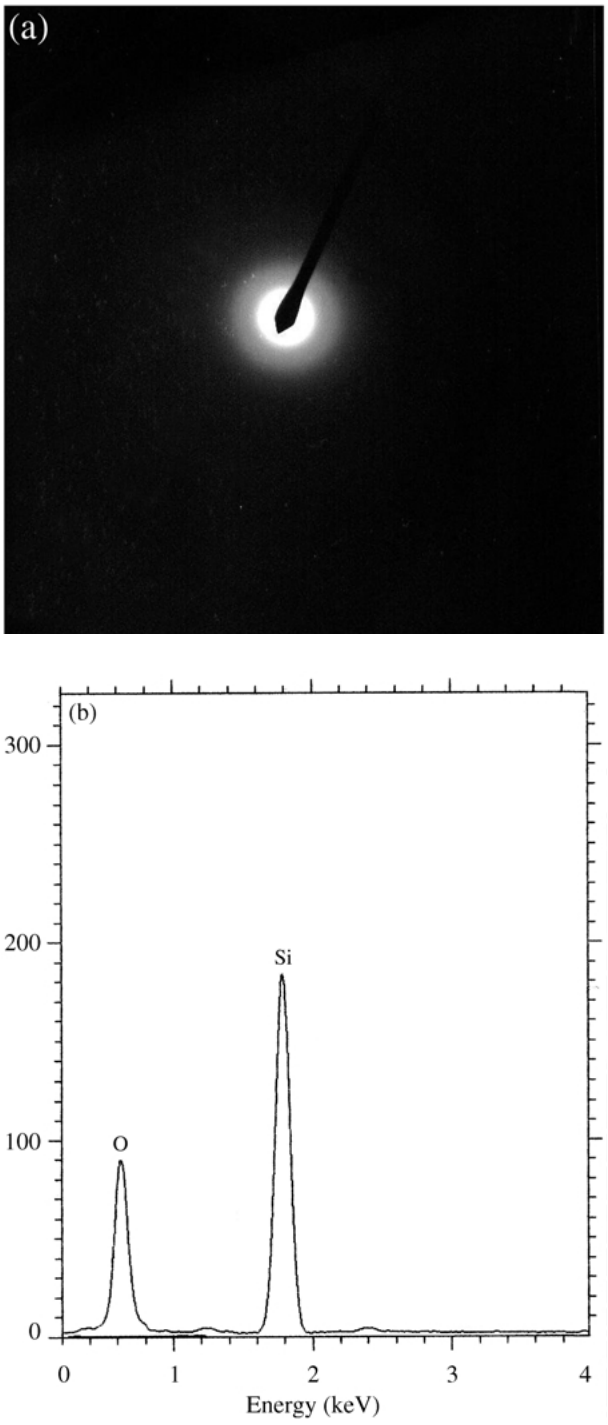

Figure 11 (a) Selected area diffraction pattern of the intermediate amorphous silica layer, (b) EDS analysis of the area.

finding suggested that the mechanism of HA-like phase formation was similar to that on silica-based bioactive materials previously studied in SBF.

A combination of chemical, structural and morphological factors were responsible for the different *in vitro* behavior of the two glass–ceramics, both with a common glass precursor.

Acknowledgments

The authors would like to thank the Local Government Generalitat Valenciana for a grant to Dr P. N. de Aza in support of a short term visit to the Materials Department, Queen Mary University of London, UK. Part of this work was supported by CICYT under project No MAT2000-0941.

References

1. T. KOKUBO, S. ITO, M. SHIGEMATA, S. SASKKA and T. YAMAMURA, *J. Mater. Sci.* **22** (1987) 4067.
2. L. L. HENCH, *J. Am. Ceram. Soc.* **81** (1998) 1705.
3. M. JARCHO, *Clin. Orthop. Relat. Res.* **157**(6) (1981) 259.
4. D. F. WILLIAMS, in ''Biocompatibility of Tissue Analogs'', edited by D. F. Williams (CRC Press, Boca Raton, FL, 1985) p. 43.
5. S. F. HULBERT, J. C. BOKROS, L. L. HENCH, J. WILSON and G. HEIMKE, in ''Ceramics in Clinical Applications: Past, Present and Future in High Tech Ceramics'', edited by P. Vincenzini (Elsevier, Amsterdam, The Netherlands, 1987) p. 189.
6. R. Z. LEGEROS *Adv. Dent. Res.* **2** (1988) 164.
7. A. MEROLLI, P. TRANQUILLI LEAALI and P. L. GUIDI, *J. Mater. Sci.: Mater. Med.* **11** (2000) 219.
8. V. PERRONE and A. MEROLLI, *Nuove prospettive Terapia* **2** (1993) 27.
9. A. MEROLLI, P. L. GUIDI and P. RANQUILLI LEALI, *It. I. Orthop. Traumatol.* **22** (1996) 119.
10. E. PARK, R. A. CONDATE ER and D. T. HOELZEL *J. Mater. Sci.: Mater. Med.* **9** (1998) 643.
11. C. A. VAN BLITTERSWIJK, S. C. HESSELING, J. J. GROTE, H. K. KOERTEN, K. DE GROOT, *J. Biomed. Mater. Res.* **24** (1990) 433.
12. K. OHURA, T. NAKAMURA, T. YAMAMURO, T. KOKUBO, Y. EBISASWA and M. OKA, *ibid.* **25** (1991) 357.
13. Z. B. LUKLINSKA and W. BONFIELD, in ''Bone-Bonding Materials'', edited by P. Ducheyne, T. Kokubo and C. A. Van Blitterswijk (Reed Healthcare Communications, 1992) p. 73.
14. P. N. DE AZA, Z. B. LUKLINSKA, A. MARTINEZ, M. R. ANSEAU, F. GUITIAN and S. DE AZA, *J. Microsc-Oxforf.* **197**(1) (2000) 60.
15. P. N. DE AZA, Z. B. LUKLINSKA, M. R. ANSEAU, F. GUITIAN and S. DE AZA, *ibid.* **201**(1) (2001) 33.
16. M. WALKER, Tesis Doctoral, Universidad de Florida, 1977.
17. T. KOKUBO, T. HAYASHI, S. SAKKA, T. KITSUGI and T. YAMAMURO, *Yogyo-Kyokai-hi.* **95**(8) (1987) 785.
18. T. EBISAWA, T. KOKUBO, K. OHURA and T. YAMAMURO, *J. Mater. Sci.: Mater. Med.* **1** (1990) 244.
19. C. OHTSUKI, T. KOKUBO and T. YAMAMURO, *J. Non-Crystal. Solids* **143** (1992) 84.
20. L. L. HENCH and J. W. WILSON, *Science* **226** (1984) 630.
21. H. ISHIZAWA, M. FUJINO and M. OGINO, in ''Handbook of Bioactive Ceramics'', edited by T. Yamamuro, L. L. Hench and J. Wilson (CRC Press, Boca Raton, FL, 1990) p. 115.
22. C. OHTSUKI, Y. AOKI, T. KOKUBO, Y. BANDO, M. NEO, T. YAMAMURO and T. NAKAMURA, *Bioceramics* **5** (1992) 79.
23. L. L. HENCH, *J. Am. Ceram. Soc.* **74** (1991) 1487.
24. T. KOKUBO, S. ITO, T. HUANG, T. HAYASHI, M. SHIGEMATA, S. SASKKA, T. KITSUGI and T. YAMAMURA, *J. Biomed. Mater. Res* **24** (1999) 331.
25. L. L. HENCH, R. J. SPLINTER, T. K. GREENLE and W. C. ALLEN, *ibid.* **2** (1971) 117.
26. W. CAO and L. L. HENCH, *Ceram Int.* **22** (1996) 493.
27. T. NONAMI and S. TSUTSUMI, *J. Mater. Sci.: Mater. Med.* **10** (1999) 475.
28. H. M. KIM, F. MIYAJI, T. KOKUBO, C. OHTSUKI and T. NAKAMURA *J. Am. Ceram. Soc.* **78** (1995) 1769.
29. H. BRÖMEL, K. DEUTSCHER, B. BLENKE, E. PFEIL and V. STRUNA *Sci. Ceram.* **9** (1977) 219.
30. T. KOKUBO, S. ITO, S. SAKKA and Y. YAMAMURO, *J. Mater. Sci.* **21** (1986) 536.
31. J. J. SHYU and J. M. WU, *J. Am. Ceram. Soc.* **73** (1990) 1062.
32. J. J. SHYU and J. M. WU, *J. Ma. Sci.* **29** (1994) 3167.
33. T. KITSUGI, T. YAMAMURO, T. NAKAMURA and T. KOKUBO, *J. Biomed. Mater. Res.* **23** (1989) 631.
34. J. D. SANTOS, L. J. JHA, F. J. MONTEIRO, *J. Mater. Sci.: Mater. Med.* **7** (1996) 181.
35. P. N. DE AZA, C. M. LOPEZ, F. GUITIAN and S. DE AZA, *J. Am. Ceram. Soc.* **76**(4) (1993) 1052.

36. P. N. DE AZA, Z. B. LUKLINSKA, M. R. ANSEAU, F. GUITIAN and S. DE AZA, *J. Microsc-Oxford* **182** (1996) 24.
37. P. N. DE AZA, F. GUITIAN, S. DE AZA and F. J. VALLE, *The Analyst* **123** (1998) 81.
38. J. GAMBLE, in ''Chemical Anatomy, Physiology and Pathology of Extracellular Fluid'' (Harvard University Press, Cambridge, 1967)
39. P. N. DE AZA, F. GUITIAN and S. DE AZA, *Scr. Metall. Mater.* **31** (1994)1001.
40. P. N. DE AZA, F. GUITIAN and S. DE AZA, in ''Advances in Science and Technology, 12. Materials in Clinical Application'', edited by P. Vincenzini (Techna Srl., 1995) p. 19.
41. P. N. DE AZA, F. GUITIAN and S. DE AZA, *Biomaterials* **18** (1997) 1285.
42. A. MERLOS, I. GRACIA, C. CANÉ, J. ESTEVE, J. BARTROLI and C. JIMENEZ, in ''Proceedings of the 5th Conference on Sensors and their Applications'' (Edinburgh, UK, 1991) p. 127.
43. P. N. DE AZA, F. GUITIAN, M. MERLOS, E. LORA-TAMAYO and S. DE AZA, *J. Mater. Sci.: Mater. Med.* **7**(7) (1996) 399.
44. R. A. ROBINSON, *J. Bone Joint Surg. Am.* **34** (1952) 389.
45. T. W. SPECHMAN and W. P. NORRIS, *Science* (1957) 126.
46. G. DACULSI, R. Z. LEGEROS, M. HEUGHEBAERT and I. BARBIEUX, *Calcif. Tiss. Int.* **46** (1990) 20.
47. G. DACULSI, R. Z. LEGEROS and C. DEUDON, *Scanning* **4**(2) (1990) 309.
48. G. DACULSI, R. Z. LEGEROS, J. P. LEGEROS and D. MITRE, *J. Biomed. Mater. Res. App. Biomat.* **2** (1991) 147.
49. M. SPECTOR, *J. Microsc-Oxford* **103** (1975) 55.
50. B. KEREBEL, G. DACULSI and A. VERBAERE, *J. Ultrastruc. Res.* **57** (1976) 266.
51. S. JACKSON, A. G. CARTWRIGHT and D. LEWIS, *Calcif. Tissue Res.* **25** (1978) 217.
52. U. GROSS and V. STRUNZ, *J. Biomed. Mater. Res.* **14** (1980) 607.
53. U. GROSS and V. STRUNZ, in ''Clinical Applications of Biomaterials'', edited by A. J. C. Lee, T. Albrektsson and P. Branemark (John Wiley & Son, New York, 1982) p. 237.
54. U. GROSS, R. KINNE, H. J. SCHMITZ and V. STRUNZ, in ''The Response of Bone to Surface Active Glass/Glass–Ceramics'' (CRC, Critical Reviews in Biocompatibility, 1988) p. 4.

Received 29 July 2002
and accepted 21 March 2003